A supersymmetric model for lattice fermions

Huijse, L.

Chapter 7
The supersymmetric model on 2 and 3 leg ladders

7.1 Ladder models as a first step towards 2D systems

In the previous chapters, we have seen, first of all, that we have a detailed understanding of the supersymmetric model on the chain and second of all, that there are numerous results for counting ground states in two dimensional systems. Where the chain has only a doubly degenerate ground state, two dimensional systems typically enjoy an exponential degeneracy. For the chain, however, our understanding extends far beyond the ground state structure, whereas such understanding is lacking for the two dimensional systems. In this chapter we consider a variety of ladder models, which will bring these two results together. On the one hand, we will see that these ladder models also exhibit superfrustration, which we typically interpret as a feature of the two dimensional systems. On the other hand, however, many of the methods we used to study the chain, such as the spectral flow analysis and entanglement entropy computations, carry over to these ladder systems. In this chapter we focus on the analysis of the ladder models. In the next chapter, however, we will discuss an interpretation of these findings for the fully two dimensional systems (see also [34, 85]).
In the first section, we discuss the ground state structure of certain 2 and 3 leg ladders. We will show in particular that these ladders typically have an extensive ground state entropy and that the ground states are in one-to-one correspondence with tilings. In section 7.3 we discuss the results of the spectral flow analysis for these models [34] and present compelling evidence for criticality in these systems. In the final two sections, we discuss the zig-zag ladder and the square ladder in more detail. The zig-zag ladder is a very rich model, with zero energy ground states at all rational fillings between 1/5 and 1/4 filling. We build up a picture, where the system is in a gapped, charge ordered phase away from 2/9 filling, whereas at this critical filling the system shows a gapless phase. There will be a strong connection between this picture and the tilings corresponding to the ground states. The square ladder on the other hand, shows remarkable similarities to the model on the chain, but there also seem to be significant differences leading to some interesting open questions.

7.2 Ground states and tilings

In the previous chapter we have seen that for the square lattice there is an explicit relation between zero energy ground states of the supersymmetric model and tilings. This relation is not exclusive to the square lattice, but seems to be a more generic feature. In chapter 5, we discussed the work of Jonsson [39] which relates homology elements of Q to tilings for the triangular and hexagonal lattice. Furthermore, we will see in this section that the ground states of the kagome ladder can also be related to tilings [21]. In the second part

of this section, we will discuss ladder realizations of the square lattice. We will show that theorem 2 also holds for these lattices, even though, their periodicities differ from the ones for which the proof was given. This is explicit support for the conjecture that theorem 2 holds for all periodicities on the square lattice.

7.2.1 Kagome ladder

In this section we consider the kagome ladder (see Fig. 7.1). This ladder has an extensive ground state entropy and the ground states can be related to tilings of the ladder. The cohomology can be computed exactly for open boundary conditions. We find a closed expression for the ground state partition function and a window of filling fraction for the supersymmetric ground states, which can both be interpreted in terms of tilings. For periodic boundary condition, the cohomology problem has not been solved, but we do have a conjecture for the ground state partition function.
Computing the cohomology in this case is slightly involved. First of all, we cannot choose the sublattice S_2 such that it consists of disconnected sites, which by themselves have zero cohomology. Instead the convenient choice for the sublattice S_2 is less trivial. The second complication arises because not all elements of the cohomology H_{12} will have the same fermion-number, which was a sufficient condition for the tic-tac-toe lemma to hold. We compute the cohomology step by step. For each step there is a supporting picture in Fig. 7.2. **Step 1** is to map the kagome ladder with hard-core fermions to a square ladder with hard-core dimers. This mapping is one-on-one. In **Step 2** we define the sublattices S_1 and S_2. **Step 3** is to note that the cohomology of one square plus one additional edge vanishes. To do so, first note that if site 3 and 4 are both empty, we get zero cohomology due to site 5 which can now be both empty and occupied. The remaining four configurations are easily shown to be either Q of something (exact) or not in the kernel of Q (not closed). **Step 4** is to build up the ladder by consecutively adding blocks with 3 rungs (9 edges) to the ladder. From step 3 we now conclude that there are only two allowed configurations for the additional S_1-sites: they must be either both empty or both occupied, since if just one of them is occupied the remaining configurations on the additional S_2-sites are exactly the ones of step 3. A simple computation shows that if both sites on S_1 are occupied, H_{Q_2} has one non-trivial element with one dimer and if both sites on S_1 are empty, H_{Q_2} has two non-trivial elements, both with two dimers.
Now it is important to note that on the three additional rungs we find three non-trivial elements of the H_{12}, but two of them have $f_2 = 2$ and one has $f_2 = 1$. It can be shown that all three indeed belong to H_Q by going through the spectral sequence step by step. This is a tedious computation, but it can be done.
Finally, we find the cohomology of the kagome ladder with open boundary conditions of length n, which corresponds to a ladder with $n + 1$ rungs and $3n + 1$ edges in total, by

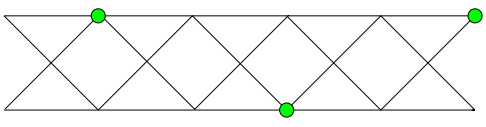

Figure 7.1: Hard-core fermions on the kagome ladder.

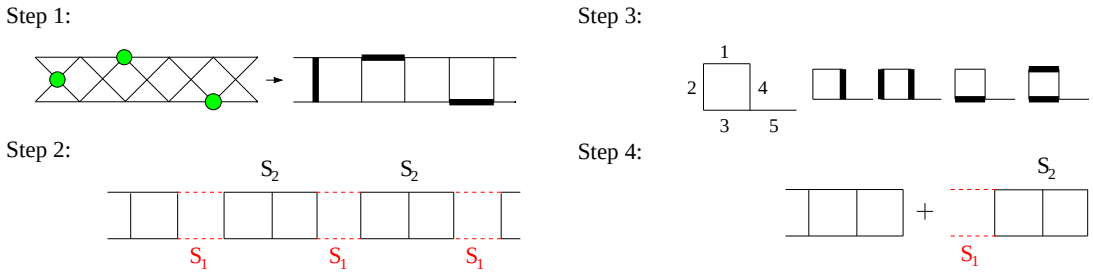

Figure 7.2: Step-by-step computation of the cohomology of the kagome ladder.

recursively adding rungs to the system. We thus obtain a recursion relation for the ground-state generating function $P_n(z) = \mathrm{tr}_{\mathrm{GS}}(z^F)$, which gives the Witten index for $z = -1$ and the total number of ground states for $z = 1$:

$$P_{n+3}(z) = 2z^2 P_n(z) + z^3 P_{n-1}(z),$$

with $P_0 = 0$, $P_1 = z$, $P_2 = 2z^2$, $P_3 = z^3$. If we introduce the following notation

$$A(n,m) = \begin{pmatrix} n-m \\ 3n-4m+1 \end{pmatrix} 2^{3n-4m+1}, \tag{7.1}$$

we can write the ground state partition sum in closed form

$$P_n(z) = \Sigma_m [A(n,m) + A(n+2, m+1)] z^m$$

Instead of drawing conclusions from here, let us picture the above in terms of tiles. From step 4 we conclude that we can cover the ladder with three tiles, two of size 9 (i.e. 9 edges) containing 2 dimers and one of size 12 containing 3 dimers. From this picture we obtain the same recursion relation provided that we allow four initial tiles corresponding to the initial conditions of the recursion relation above. Furthermore, we can see directly that the window of filling fraction of the tiles runs from 2/9 to 1/4. Using the recursion relation, we find that the ground state entropy is set by the largest solution $\lambda_{\max}$ of the characteristic polynomial $\lambda^4 - 2\lambda - 1 = 0$, giving $S_{\mathrm{GS}}/L = (\ln \lambda_{\max})/3 = 0.1110\ldots$.
For the case of periodic boundary conditions, the full cohomology problem has not been solved. However, we do conjecture an expression for the ground state partition sum, that has been verified numerically for systems up to 33 sites. First we compute the cohomology for an open ladder with an extra leg on the lower rung on each side. For this system, we prove that the ground state generating function satisfies

$$Q_n(z) = 2z^2 Q_{n-3}(z) + z^3 Q_{n-4}(z).$$

For the closed ladder of length n (with n rungs and $3n$ sites), we now naively constructed the following recursion relation

$$X_n(z) = P_{n-1}(z) + 2z Q_{n-3}(z) + z^2 P_{n-3}(z). \tag{7.2}$$

However upon comparison with the numerical data we conclude that it gives the Witten index correctly, but it overcounts the number of ground states. We conjecture that when

the first and second term in (7.2) differ by one power in z, these states are actually superpartners and similarly for the second and third term in (7.2). These terms should thus be subtracted. Using the definition (7.1), we can write

$$Q_n(z) = \Sigma_m A(n+4, m+2) z^m$$

and we find that the conjectured form of the ground state partition sum for the closed ladder is

$$\begin{aligned} X_n(z) = \Sigma_{m=0}^n [&A(n-1,m) + A(n+1,m+1) + 2zA(n+1,m+2) \\ &+ z^2 A(n-3,m) + z^2 A(n-1,m+1)] z^m \\ -\Sigma_{m=0}^n \mathrm{Min}[&A(n-1,m) + A(n+1,m+1), A(n+1,m+2)](z^m + z^{m+1}) \\ +\Sigma_{m=0}^n \mathrm{Min}[&A(n+1,m+2), A(n-3,m) + A(n-1,m+1)](z^{m+1} + z^{m+2}). \end{aligned}$$

7.2.2 Ladder realizations of the square lattice

As we mentioned in the beginning of this chapter, the main focus here is on ladder realizations of the square lattice. We construct ladders from the square lattice by choosing the periodicity $\vec{u} = (L, 0)$ in the horizontal direction, and for the periodicity $\vec{v}$ we consider the three cases $\vec{v} = (0, 2)$, $\vec{v} = (1, 2)$ and $\vec{v} = (3, 3)$ (see figure 7.3). The first two are 2 leg ladders, the first being the simple square ladder and the second turns out to be a zig-zag ladder. The third is a 3 leg ladder and is clearly the most two dimensional, in the sense that the particles can really hop past each other in this lattice.

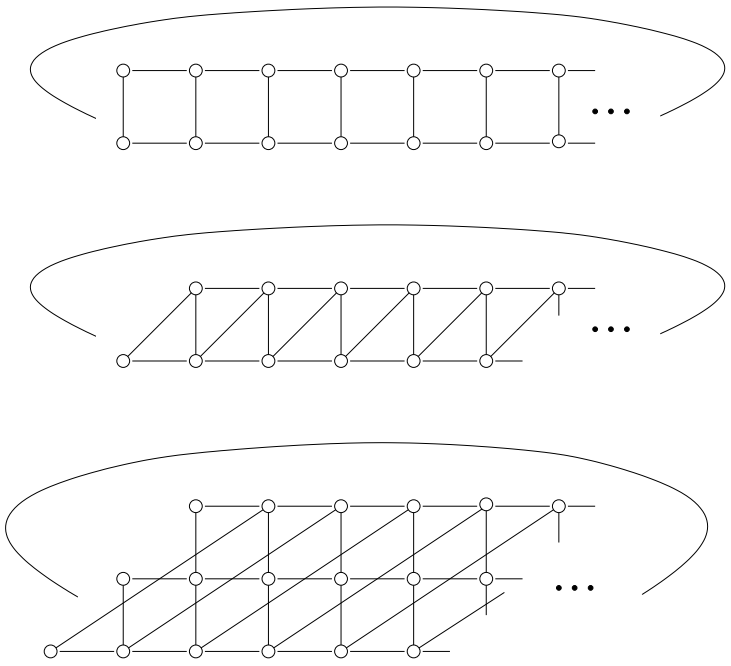

Figure 7.3: From top to bottom we show the square ladder, the zig-zag ladder and the 3 leg ladder, obtained from the square lattice by imposing the periodicities $\vec{u} = (L, 0)$ in the horizontal direction and $\vec{v} = (0, 2)$, $\vec{v} = (1, 2)$ and $\vec{v} = (3, 3)$ respectively in the vertical direction.

In the previous chapters, we discussed theorem 2 which relates ground states to tilings for the supersymmetric model on the square lattice with doubly periodic boundary conditions.

We strongly believe this theorem for all periodicities, however, a proof was given only for the case $\vec{u} = (m, -m)$ and $v_1 + v_2 = 3p$. It follows that the theorem has been proven only for zig-zag ladders of length $L = 3k$ and for the 3 leg ladder with length $L = 3k$. Although the square ladder falls outside the class of tori for which we prove the theorem, we can quite easily extend the proof for this case. Before we give the proof, we should mention that for all three ladders with up to 32-36 sites (depending on the model), the numerics are in precise agreement with the theorem. Clearly, this is very strong support for our belief that the theorem holds in general.

Square ladder

For the square ladder ($\vec{u} = (L, 0)$ and $\vec{v} = (0, 2)$) the Witten index follows directly from Jonsson's theorem [37] (see theorem 1 in this thesis). For length $L = 4k$ we find that there are 4 tilings with k tiles using just the diamonds, for length $L \neq 4k$ there are no tilings. Using the fact that $-(-1)^d \theta_d \theta_{d^*} = \pm 1$ for $L = 2k + 1$ and $L = 2k$ respectively, we find

$$W = \begin{cases} 3 & \text{for } L = 4k \\ -1 & \text{for } L = 4k + 2 \\ 1 & \text{for } L = 4k \pm 1 \end{cases}$$

For the case with $L = 4k$, we easily prove that there are 3 ground states with $2k$ fermions. The proof for the other cases is slightly more tedious. To compute the cohomology for $L = 4k$, we divide the lattice into two sublattices, where S_1 contains the isolated sites $(1 + 4m, 0)$ and $(3 + 4m, 1)$ with $m = 0, \ldots, k - 1$. The sublattice S_2 is then a periodic chain of length $2L - 2k = 6k$. It is easily seen that H_{Q_2} is trivial unless the S_1 sites are all empty or all occupied. The first case corresponds to two non-trivial elements at grade $2k$ (the 2 ground states on the periodic chain with $2k$ particles). The second case gives the third non-trivial element at grade $2k$. To compute H_{12} and H_Q are now trivial steps and we conclude that there are 3 ground states with $2k$ fermions for $L = 4k$. For $L = 4k + 3$ we can choose the sublattices such that S_1 consists of $2k + 2$ disconnected sites and S_2 is an open chain of length $6k + 4$. It quickly follows that the only non-trivial element of H_2 has all sites on S_1 occupied and thus that there is a unique ground state with $2k + 2$ particles (in agreement with $W = +1$). For $L = 4k + 1$ we can choose the sublattices such that S_1 consists of $2k - 1$ disconnected sites and 2 connected sites and S_2 is a periodic chain of length $6k + 1$. The configuration with all S_1 sites empty gives one non-trivial element of H_2 at grade $2k$, all other allowed configurations on S_1 give trivial elements of H_2. It follows that there is a unique ground state with $2k$ particles (in agreement with $W = +1$). Finally, for $L = 4k + 2$ we can choose the sublattices such that S_1 consists of $2k + 1$ disconnected sites and S_2 is a periodic chain of length $6k + 2$, with one extra site connected to it. All configurations with at least on particle on S_1 are trivial elements of H_2. All S_1 sites empty gives rise to a periodic chain of length $6k + 2$, with one extra site connected to it. Using the 'tic-tac-toe' lemma for this case, where the extra site is considered as the S_1 sublattice one easily proves that there is one ground state with $2k+1$ particles. We conclude that for $L = 4k + 2$, there is a unique ground state with $2k + 1$ particles (in agreement with $W = -1$).

Zig-zag ladder

For the zig-zag ladder ($\vec{u} = (L, 0)$ and $\vec{v} = (1, 2)$) the Witten index also follows from Jonsson's theorem. However, counting the number of tilings is less trivial than for the square ladder. The zig-zag ladder nicely accommodates tiling configurations. In the short direction the boundary condition is $\vec{v} = (1, 2)$, which is precisely along the edges of one of the diamonds and one of the squares. It follows that we can tile the zig-zag ladder with precisely one row of tiles, using just these two tiles that fit the boundary conditions. Imposing the periodicity $\vec{v} = (1, 2)$ changes the shape of the tiles. This is depicted in figure 7.4.

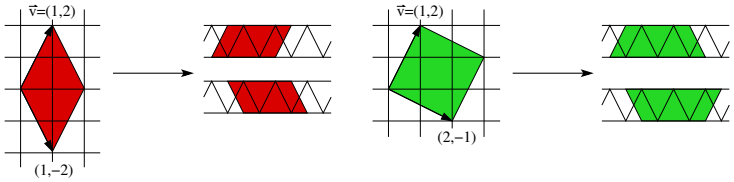

Figure 7.4: Two of the four allowed tiles nicely fit the periodicity imposed by $\vec{v} = (1, 2)$. We show what these tiles look like on the zig-zag ladder. Both the diamond as well as the square turn into two tiles on the zig-zag ladder differing in their orientation.

For the zig-zag ladder with N sites and open boundary conditions the generating function for tiling configurations is

$$P^o_N(z) = zP^o_{N-4}(z) + zP^o_{N-5}(z), \tag{7.3}$$

with $P^o_1 = 0$, $P^o_2 = 0$, $P^o_3 = 0$ and $P^o_4 = z$. Interestingly, this recursion relation also seems to hold for the ground state generating function. This has been checked numerically for up to 22 sites. The only difference is that the first couple of values of P^o are different: $P^o_1 = 0$, which is also true for the tilings, but $P^o_2 = z$, $P^o_3 = 2z$ and $P^o_4 = 2z$. It follows that the difference between the number of tilings and the number of ground states diverges as a function of N, due to a propagating different offset.
For the zig-zag ladder with periodic boundary conditions the generating function for tiling configurations obeys the same recursion relation (7.3). In this case, however, we also have an expression in closed form for the number of tilings

$$R_{\vec{u},\vec{v}}(z) = 4z^{L/2}(1-q) + \sum_{k=1}^{(L+5q)/10} z^{\tilde{L}-k+1} \frac{L}{2k-q} \begin{pmatrix} \tilde{L}-k \\ 4k-1-2q \end{pmatrix}$$

with $q = L \mod 2$ and $\tilde{L} = L/2 - 1 + q/2$, where L is the length of the ladder (so the number of sites is $N = 2L$).
From theorem 2 we know that for $L = 3k$ the ground state partition function reads $Z_{\mathrm{GS}}(z) = R_{\vec{u},\vec{v}} + (-1)^{(\theta_{2k}+1)} 2z^{[4k/3]}$, with $[a]$ the nearest integer to a and

$$\theta_d \equiv \begin{cases} 2 & \text{if } d = 3k, \text{ with } k \text{ integer} \\ -1 & \text{otherwise.} \end{cases} \tag{7.4}$$

Numerically we verified the following expression for general $L = N/2$ up to $N = 34$

$$Z_{\mathrm{GS}}(z) = R_{\vec{u},\vec{v}} - (-1)^{(\theta_{d^*}+[2N/9])} \theta_{d^*} z^{[2N/9]}, \tag{7.5}$$

with $d^* = \gcd(u_1 + u_2, v_1 + v_2) = \gcd(L, 3)$.

3 leg ladder

For the 3 leg ladder ($\vec{u} = (L, 0)$ and $\vec{v} = (3, 3)$) the theorem for the number of ground states is proven for $L = 3k$. The number of tilings can be expressed as

$$R_{\vec{u},\vec{v}}(z) = \sum_{s \geq L/9}^{2L/9} 9 \binom{L/3}{2L/3 - s} z^{2L/3},$$

with the restriction that s is integer and that $\binom{a}{b} = 0$ if a and/or b are not positive integers. It follows that for $L \neq 3k$, there are no tilings. Furthermore, we see that for $L = 3k$ there are only tilings with $2L/3 = 2k$ tiles, more precisely with k diamonds and k squares.
From theorem 1 for the Witten index, we find

$$W = \begin{cases} -(-1)^L & \text{for } L \neq 3k \\ -(-1)^L 4 + R_{\vec{u},\vec{v}}(z = -1) & \text{for } L = 3k. \end{cases}$$

For $L \neq 3k$ we can thus quickly conjecture that $\Delta = 1$ in theorem 2, since the number of ground states must be positive. For $L = 3k$ we conjecture from comparison with numerical results for up to $L = 12$ that $\Delta = -(-1)^k 4$.

7.3 Spectral flow for ladder realizations of the square lattice

To investigate criticality of the supersymmetric model on ladder realizations of the square lattice, we investigated how the spectrum changes upon twisting the boundary condition along the $(L, 0)$-direction from periodic to anti-periodic [34]. This method was described and the results discussed for the supersymmetric model on the chain in section 4.8. It is a powerful way of distinguishing between critical and gapped states: for a gapped state, the correlation length is finite and a change in the boundary conditions will have an exponentially small effect on the energy. In contrast, for a critical state the change in the energy will be substantial since the correlation length goes to infinity. More specifically, the energy has a parabolic dependence on the boundary twist.
In addition to this, one can extract more quantitative properties from twisting the boundary condition. This is described in detail in section 4.8, but will be briefly summarized here for convenience. For a critical supersymmetric system in 1D with a Fermi surface, we expect that its continuum limit is described by an $\mathcal{N}$=2 superconformal field theory (SCFT). In such a theory, twisting the boundary condition corresponds to going from the Ramond to the Neveu-Schwarz sector. The twist can be carried out continuously and leads to a spectral flow [49]. If we define the twist parameter α to be integer in the Ramond sector and half-integer in the Neveu-Schwarz sector, the energy is a parabolic function of α,

$$E_\alpha = E_{\alpha=0} + \alpha \tilde{Q}_{\alpha=0} + \alpha^2 c/3, \tag{7.6}$$

where c is the central charge. $\tilde{Q}_\alpha \equiv q_L + q_R$ is the sum of the left- and right-moving U(1) charges and depends linearly on α [49, 43]. Their difference is conserved under the twist

and is related to the fermion number. In the lattice model, we can go from periodic to anti-periodic boundary conditions continuously by adding a phase to the terms that hop a particle over the boundary, e.g. $c_N^\dagger c_1 +$ h.c. is replaced by $e^{2\pi\imath\alpha} c_N^\dagger c_1 +$ h.c. The eigenvalues of the translation operator p_α will now depend linearly on the twist parameter:

$$T_\alpha^L |\psi\rangle \quad = \quad e^{2\pi\imath p_0 L} e^{2\pi\imath\alpha F} |\psi\rangle \equiv e^{2\pi\imath p_\alpha L} |\psi\rangle, \tag{7.7}$$

so $p_\alpha = p_0 + \alpha F/L$ where L is the length of the system and F is the total number of particles in the state $|\psi\rangle$.
We computed the spectrum for various values of the twist parameter via exact diagonalization. We find that the majority of states have a parabolic dependence on the twist parameter by fitting a parabola to the energy levels as a function of the twist parameter, or equivalently, as a function of p_α. This clearly indicates that the system is critical. An example is shown in fig. 7.5.
For a critical system, the energy of the SCFT in (7.6) is related to the numerically obtained value of the energy via $E_{\text{num}} = 2\pi E_{\text{CFT}} v_F / L$, where v_F is the Fermi velocity and L the system size. So by comparing the parabolic fit to the numerics with equation (7.6), we can obtain the ratios E_α/c and $\tilde{Q}_\alpha/c$.

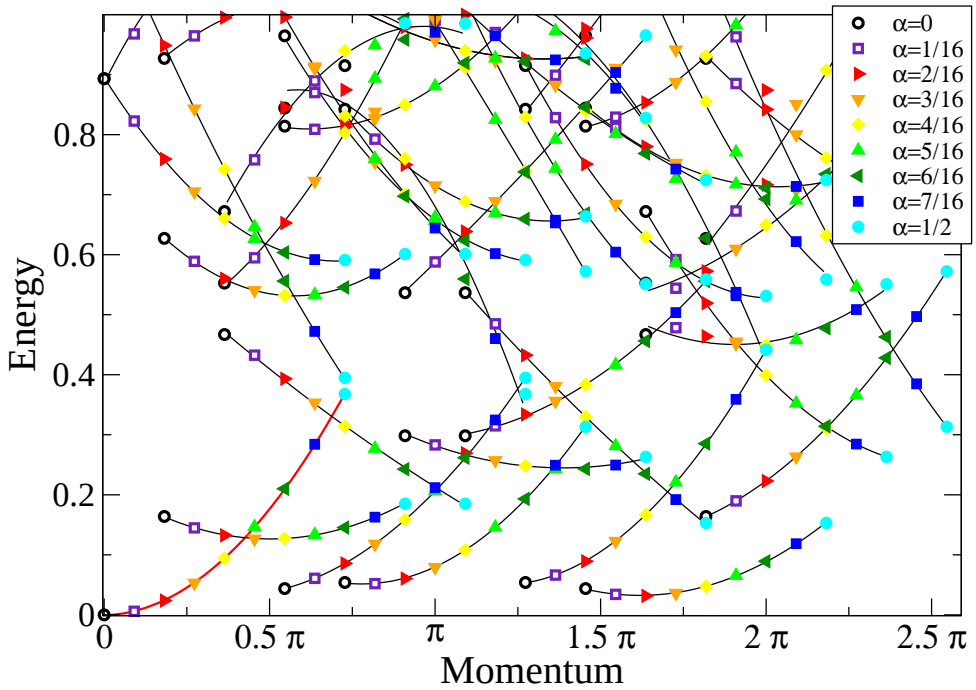

Figure 7.5: In the plot we show nine energy spectra as a function of momentum for increasing values of the twist parameter ($0 \leq \alpha \leq 1/2$, with steps of $1/16$) for a system with 33 sites ($\vec{u} = (11, 0)$ and $\vec{v} = (3, 3)$) and 8 fermions. The lines are parabolic fits to the numerical data. The results from the spectral flow analysis for the red line through the origin appear in red in table 7.1.

We extracted values for E_α/c and $\tilde{Q}_\alpha/c$ via the above described method for three models with up to 36 sites (see table 7.1). For the lowest energy levels, we typically find that $(E/c, \tilde{Q}/c)$ in the NS sector is either $(-1/12, 0)$, $(1/12, 1/3)$ or $(1/4, 2/3)$, all with an accuracy of within 10%. These values occur in the Kac table for the k-th minimal model

Table 7.1: Results from spectral flow analysis for three types of tori $(L,0)\times\vec{v}$ (and $(L,-1)\times(1,2)$ for the zig-zag ladder with odd number of sites wrapped on a Möbius strip). Here, N denotes the number of sites and F the number of fermions. We show the results for the lowest energy level for each system. The values for E and $\tilde{Q}$ are given in the Neveu-Schwarz sector ($\alpha=1/2$) and c is the central charge. For the level in red boldface the results are extracted from the red line in fig. 7.5.

N	$\vec{v}$	F	E/c	$\tilde{Q}/c$
18	$(3,3)$	4	-0.0851	0.004
36	$(3,3)$	8	-0.0841	-0.002
15	$(3,3)$	4	0.0898	0.349
21	$(3,3)$	4	0.0850	0.337
24	$(3,3)$	5	0.0850	0.337
30	$(3,3)$	7	0.0853	0.338
33	**(3,3)**	**8**	**0.0855**	**0.338**
9	$(1,2)$	2	-0.0858	-0.005
18	$(1,2)$	4	-0.0842	-0.002
27	$(1,2)$	6	-0.0839	-0.001
17	$(1,2)$	4	0.0844	0.336
26	$(1,2)$	6	0.0840	0.335
35	$(1,2)$	8	0.0839	0.335
14	$(1,2)$	3	0.2666	0.701
23	$(1,2)$	5	0.2458	0.657
32	$(1,2)$	7	0.2432	0.652
16	$(0,2)$	4	-0.0897	-0.014
24	$(0,2)$	6	-0.0889	-0.012
32	$(0,2)$	8	-0.0885	-0.011
12	$(0,2)$	3	0.0911	0.350
20	$(0,2)$	5	0.0900	0.348
28	$(0,2)$	7	0.0894	0.347
14	$(0,2)$	4	0.0855	0.338
22	$(0,2)$	6	0.0849	0.337
30	$(0,2)$	8	0.0847	0.336

of an $\mathcal{N}=(2,2)$ superconformal field theory with k even [43]. This can be seen as follows. The possible values of the conformal dimensions and corresponding $U(1)$ charges of the superconformal minimal models are given in section 3.4. In the Neveu-Schwarz sector they read

$$h_{p,r}(k)=\frac{p(p+2)-r^2}{4(k+2)}\qquad q_r(k)=\frac{r}{k+2},$$

with $p=0,1,\ldots,k$ and $r=-p,-p+2,\ldots,p-2,p$. For a state with $h_L=h_R=h_{p,r}(k)$ and $q_L=q_R=q_r(k)$, we find

$$\begin{aligned}\frac{E}{c} &= \frac{2h_{p,r}(k)}{c}-\frac{1}{12}=\frac{p(p+2)-r^2-k/2}{6k}\\ \frac{\tilde{Q}}{c} &= \frac{2q_r(k)}{c}=\frac{2r}{3k}.\end{aligned}$$

One easily verifies that with $p = r = 0$, $p = r = k/2$ and $p = r = k$, we find $(E/c, Q/c) = (-1/12, 0)$, $(1/12, 1/3)$ and $(1/4, 2/3)$ respectively. The fact that we obtain these ratios from analyzing the spectral flow is very compelling evidence that each of these systems is quantum critical.

A few remarks are in order. The fits become less reliable for levels with higher energies, but also if there is an avoided level crossing as a function of the twist. This happens when the energy levels in the Ramond or NS sector are degenerate. For the chain, the avoided crossings vanish in the continuum limit (see section 4.8.1), so one would expect that for the other models this is also merely a finite size feature. For the square ladder ($\vec{u} = (L, 0)$ and $\vec{v} = (0, 2)$), however, the results from exact diagonalization suggest that the avoided crossing will prevail for large system sizes. We will discuss this issue in more detail in section 7.5.

For the zigzag ladder ($\vec{u} = (L, 0)$ or $\vec{u} = (L, 1)$ (Möbius strip) and $\vec{v} = (1, 2)$), we find that the energy depends parabolically on the boundary twist for filling fractions close to 2/9 filling. However, at 1/4 and 1/5 filling we find quite a different behavior; the energy of the states does not change or hardly changes as a function of the twist parameter. This suggests that away from 2/9 filling the system is gapped. In the section 7.4, we present further evidence for this observation. If we look more carefully at the spectral flow for this system one may even argue that only the extra or missing ground states, which are not related to tilings, but correspond to Δ in theorem 2, lead to critical modes. For a nice illustration of this idea see figure 7.6. Here we plot the spectral flow for the zig-zag ladder with 27 sites on a Möbius strip at 2/9 filling, that is $f = 6$. There are 90 possible tilings with 3 diamonds and 3 squares and the system realizes 88 zero energy ground states. In the plot we clearly see, that a few ground states show critical behavior under spectral flow, whereas the bulk of the ground states hardly reacts to the boundary twist. This is even more apparent upon comparison to the spectral flow of the 3 leg ladder with 36 sites and 8 fermions, where all 50 ground states clearly show a significant reaction to the boundary twist (see figure 7.7). Of course, it is difficult, if not impossible, to identify the critical modes in the zig-zag ladder with the *missing* ground states. However, from the proof of theorem 2 it follows that of the 9 tilings with diamonds and squares alternating, only 7 correspond to cohomology elements. It follows that the 9 cross-cycles corresponding to the tilings are not independent and one may argue that this leads to 7 extended states which show the critical behavior.

7.4 Zig-zag ladder

The zig-zag ladder nicely accommodates both the diamond- as well as the square-tile and thus has zero energy ground states for all rational fillings between 1/4 and 1/5. Consequently, this model forms an ideal testing ground for investigating the tiling-ground state relation beyond counting. In the previous section we saw that the spectral flow analysis for this model indicates the presence of critical modes, but only near 2/9 filling. In this section we present further evidence that the system has a gap at 1/4 and 1/5 filling due to charge ordering. In analogy with our studies of the supersymmetric model on the chain, we investigate the entanglement entropy and one-point functions for this model. For 1/4 filling we even prove the charge ordering explicitly, because we find an analytic expression for the ground states. We suspect, although we cannot prove this,

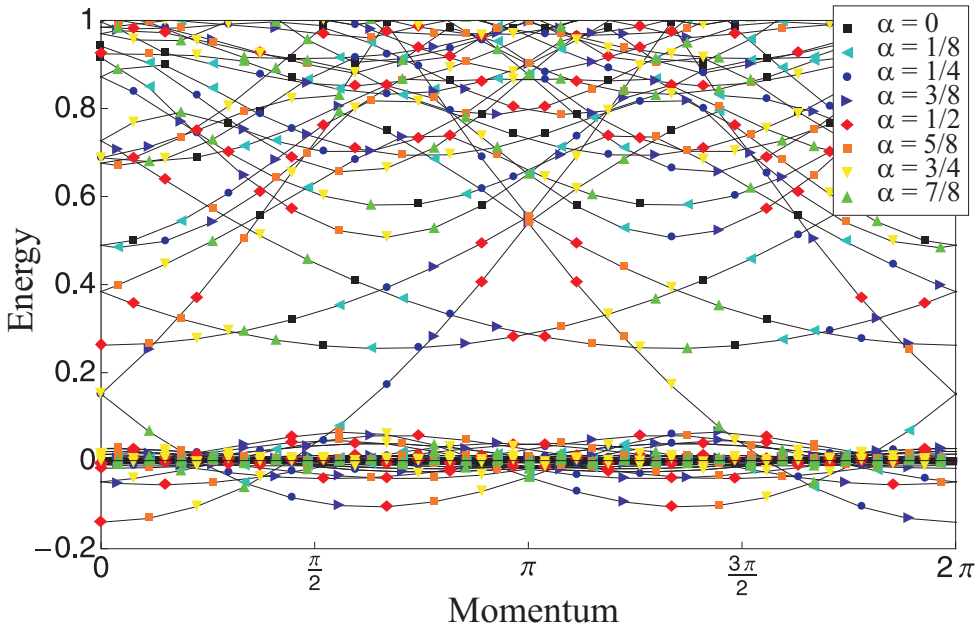

Figure 7.6: In the plot we show eight energy spectra as a function of momentum for increasing values of the twist parameter ($0 \leq \alpha \leq 7/8$, with steps of $1/8$) for the zig-zag ladder with 27 sites ($\vec{u} = (13, -1)$ and $\vec{v} = (1, 2)$) and 6 fermions. The lines connect the levels for different values of the twist parameter.

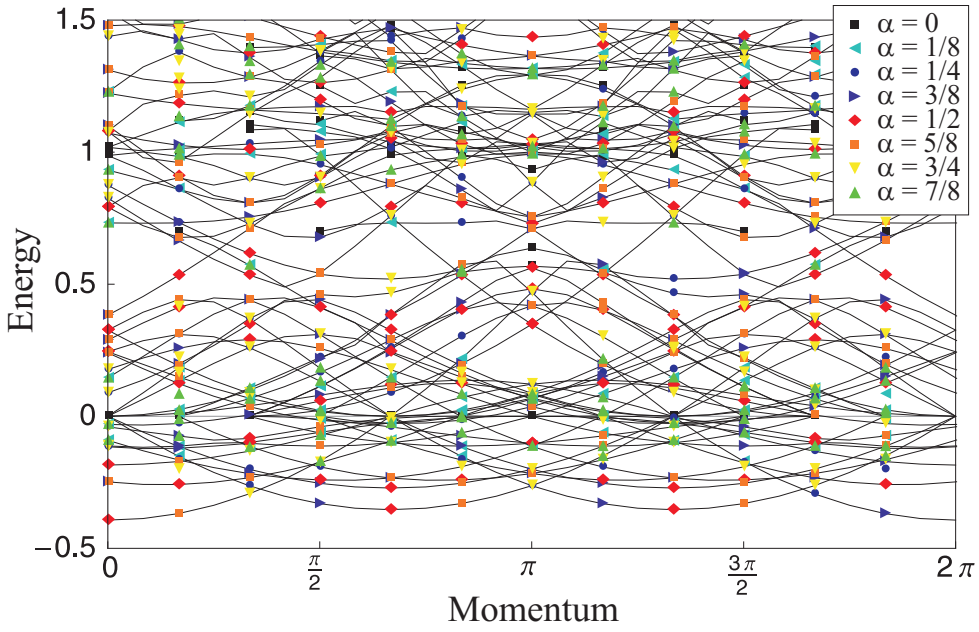

Figure 7.7: In the plot we show eight energy spectra as a function of momentum for increasing values of the twist parameter ($0 \leq \alpha \leq 7/8$, with steps of $1/8$) for a system with 36 sites ($\vec{u} = (12, 0)$ and $\vec{v} = (3, 3)$) and 8 fermions. The lines connect the levels for different values of the twist parameter.

that the spectrum of the model on the zig-zag ladder exhibits a gap everywhere except at 2/9 filling. On the one hand, this may be interpreted as a phase transition due to

competing orders (between the diamond and the squares), on the other hand, there are indications that only the extra or missing ground states, which are not related to tilings, but correspond to Δ in theorem 2, lead to critical modes. In the latter case the ground states that correspond to tilings would always exhibit a form of charge order and the critical modes arise independently.
Finally, we discuss a mapping from this model onto a spin chain. Since exploiting this relation could provide further insight in both the supersymmetric model as well as the spin chain, this may be an interesting future project.

7.4.1 Exact ground states at and near quarter filling

As we have seen in section 7.2.2 the zig-zag ladder is chosen such that it nicely accommodates tiling configurations (see figure 7.4). If the boundary condition in the horizontal direction is $\vec{u} = (2n, 0)$ with $n \in \mathbb{Z}_{\geq 1}$ there are always four tilings using only the diamonds. Now remember that one can associate a cross-cycle to a tiling (see section 5.4). It turns out that for the zig-zag ladder at quarter filling these cross-cycles are not just representatives of the homology of Q, but they are the actual ground states of the system at quarter filling[1]. A cross-cycles is a product state of one-particle-states with the particle resonating between two sites. To be precise, for general length $2n$ (boundary conditions $\vec{u} = (2n, 0)$ and $\vec{v} = (1, 2)$) the four ground states can be written as

$$\Psi_\alpha = \prod_{j=0}^{n-1} (c^\dagger_{4j+\alpha \mod 4n} - c^\dagger_{4j+\alpha+1 \mod 4n})|0\rangle, \tag{7.8}$$

where $\alpha = 0, 1, 2, 3$ and for the creation operators $c_i^\dagger$, $i = 0, \ldots, 4n-1$ with i even (odd) labelling the sites of the lower (upper) rung of the ladder (see figure 7.8). These ground state can also be written in a translational invariant form and one finds that

- for $\vec{u} = (4m, 0)$ with $m \in \mathbb{Z}$ there are two ground states at momentum $p_1 = \pi/2$ and two ground states at momentum $p_2 = 3\pi/2$, and
- for $\vec{u} = (4m + 2, 0)$ with $m \in \mathbb{Z}$ there are two ground states at momentum $p_1 = 0$ and two ground states at momentum $p_2 = \pi$.

Interestingly, we can compute the effect of a boundary twist on these states analytically. The momenta of the states change linearly with the twist as expected. But we find that the twist has no effect on the energy of the states. This can be readily understood by remembering that the ground states are product states of one particle states with the particle resonating between two sites. A change in the boundary condition can thus be absorbed locally in the state of the particle that resonates across the boundary.
If we move away from quarter filling, the ground states correspond to tilings containing both diamonds and squares. It can be easily checked that the cross-cycles corresponding to tilings containing the square tile are annihilated by $Q^\dagger$, but not by Q. It follows that there is no analytic expression available for ground states at general filling. Nevertheless, there is more evidence that the relation between ground states and tilings is very robust.

[1] There is an exception for small chain lengths ($1 \leq n \leq 4$), where either not all four cross-cycles are independent ($n = 1$) or they do not constitute a complete representation of the cohomology ($n = 2, 3, 4$) at quarter filling. For $n > 4$ these subtleties do not occur.

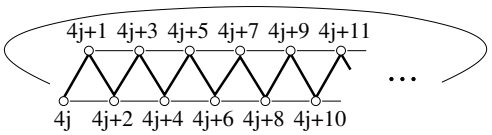

Figure 7.8: The zig-zag ladder can be obtained from the square lattice by imposing the periodicities $\vec{u} = (L, 0)$ and $\vec{v} = (1, 2)$. The sites on the lower (upper) rung are labelled by even (odd) integers.

First of all, the momenta of the ground states seem to nicely agree with the momenta one would expect from the tilings. For example at 1/5 filling the tilings are invariant under translations by 5 sites in the horizontal direction. Indeed we find that the 5 ground states at 1/5 filling have momenta $p_k = 2\pi k/5$ with $k = 1, \ldots, 5$.
Second of all, the tilings tell us that there are massless, fractionally charged defects in the system. Upon inspection of the tiles, one easily verifies that in a given tiling a sequence of 5 diamonds can be replaced by 4 squares. The new tiling has one charge less, however, since we can take the four squares apart, they can each be seen as a defect of charge $-1/4$. Note that these defects do not cost any energy.
Finally, we find an analytic expression for two states with zero energy for ladders with $\vec{u} = (4m - 1, 0)$, anti-periodic boundary conditions and $f = 2m - 1$. Clearly, this is just a curiosity (the ground state for these systems has negative energy), but for completeness we wish to mention it here. This state was found by considering the analytic ground state at quarter filling on a ladder with an odd number of rungs by leaving one rung empty. This can be seen as introducing a defect of charge $-1/2$ in the charge ordered state. We consider a ladder with $\vec{u} = (2n - 1, 0)$ and $f = n - 1$. By writing out the effect of the hamiltonian on this state (and handling the minus signs with care), one can show that for $\alpha = 0, 1$ the following states have zero energy

$$\Psi_\alpha = \sum_k (-1)^k T^k \prod_{j=0}^{n-2} (c^\dagger_{4j+\alpha} - c^\dagger_{4j+\alpha+1})|0\rangle, \tag{7.9}$$

where T is the translation operator. We now see immediately that the translation eigenvalue is $t = -1$ and since $2n - 1$ is odd, we also have $t^{2n-1} = -1$. This is only the case if we have anti-periodic boundary conditions and an odd number of fermions, so $f = 2m - 1$ and thus $\vec{u} = (4m - 1, 0)$. Consequently, we have two zero energy states at momentum $p = \pi$. This is verified numerically for ladders of up to 30 sites.

7.4.2 Entanglement entropy

For a critical system of finite size N the entanglement entropy between a subsystem A and the rest of the system is given by (see section 4.10)

$$S(l_A) = \frac{c}{3} \log\left(\frac{N}{\pi} \sin\left(\frac{l_A \pi}{N}\right)\right) + b \tag{7.10}$$

where b is some constant, c is the central charge and l_A is the size of the subsystem A.
From the spectral flow analysis, we found that the zig-zag ladder exhibits critical behavior near 2/9 filling. We have seen in section 4.10 that entanglement entropy computations are not reliable for degenerate states. Clearly for the zig-zag ladder this is a problem, since

near 2/9 filling the ground states are highly degenerate even if translational invariance is imposed. To overcome this problem we have computed the entanglement entropy in the Neveu-Schwarz sector. In particular, we select precisely the states which exhibit the critical behavior under spectral flow.
We computed the entanglement entropy for the zig-zag ladder with even ($\vec{u} = (L, 0)$ and $\vec{v} = (1, 2)$) and odd ($\vec{u} = (L, -1)$ and $\vec{v} = (1, 2)$) number of sites. For the states we selected using the spectral flow analysis we find a nice fit with the formula for the entanglement entropy using b and c as fit parameters (see figure 7.9). The inset in the figure shows the fitted values for c. The values suggest that the central charge is smaller than 3 which is in agreement with the minimal models for which $1 \leq c < 3$. However, the size of the studied systems is clearly too small to draw more quantitative conclusions on the value of the central charge.
We find that for the entanglement entropy of ground states at 1/4 and 1/5 filling, there is no good fit with (7.10). In fact, we find that the entanglement entropy saturates. This implies that the correlation length is finite and thus the ground states at 1/4 and 1/5 filling are not critical. Nice examples are shown in figures 7.10(b) and 7.10(a). Clearly, for the ground state at 1/4 filling, we know that the correlation length is finite, since the ground state is a product state. In particular, if we define n_c as the number of resonating bonds that is cut by the boundary between subsystem A and the rest of the system, we find that the entanglement entropy of the states $|\Psi_\alpha\rangle$ (7.8) reads

$$S_E = \begin{cases} 0 & \text{if } n_c = 0, \\ \ln 2 & \text{if } n_c = 1, \\ 2 \ln 2 & \text{if } n_c = 2. \end{cases}$$

In figure 7.10(b) we clearly see that, apart from the two boundary points, the entanglement entropy has one of two values, depending on whether the subsystem size is even or odd. Here the entanglement entropy is computed for one of the two translationally invariant ground states with momentum $p = \pi/2$. This state is a translationally invariant superposition of the states $|\Psi_\alpha\rangle$. Since not all $|\Psi_\alpha\rangle$ are completely orthogonal, it is not so easy to compute the entanglement entropy analytically for such a superposition. However, it is clear that in such a ground state the possibility to have zero entanglement entropy, drops out. Upon further inspection, one can probably explain the numerical result in more detail, however, it is not so clear what one learns from this.

7.4.3 Charge order at quarter and one fifth filling

The four ground states of the zig-zag ladder at quarter filling show a clear form of charge ordering. From the analytic expressions for the ground states (7.8) one easily obtains that the one-point functions, $< n_k >_\alpha \equiv \langle \Psi_\alpha | c_k^\dagger c_k | \Psi_\alpha \rangle$, read

$$< n_k >_\alpha = \begin{cases} 0 & \text{for } k - \alpha = 0 \mod 4 \text{ and } k - \alpha = 1 \mod 4, \\ 1/2 & \text{for } k - \alpha = 2 \mod 4 \text{ and } k - \alpha = 3 \mod 4, \end{cases}$$

where $\alpha = 0, 1, 2, 3$ labels the four ground states.
Both the spectral flow analysis as well as the entanglement entropy computations for the zig-zag ladder at 1/5 filling indicate that the system is also gapped in that regime. By numerically computing one-point functions for the zig-zag ladder, we investigate if

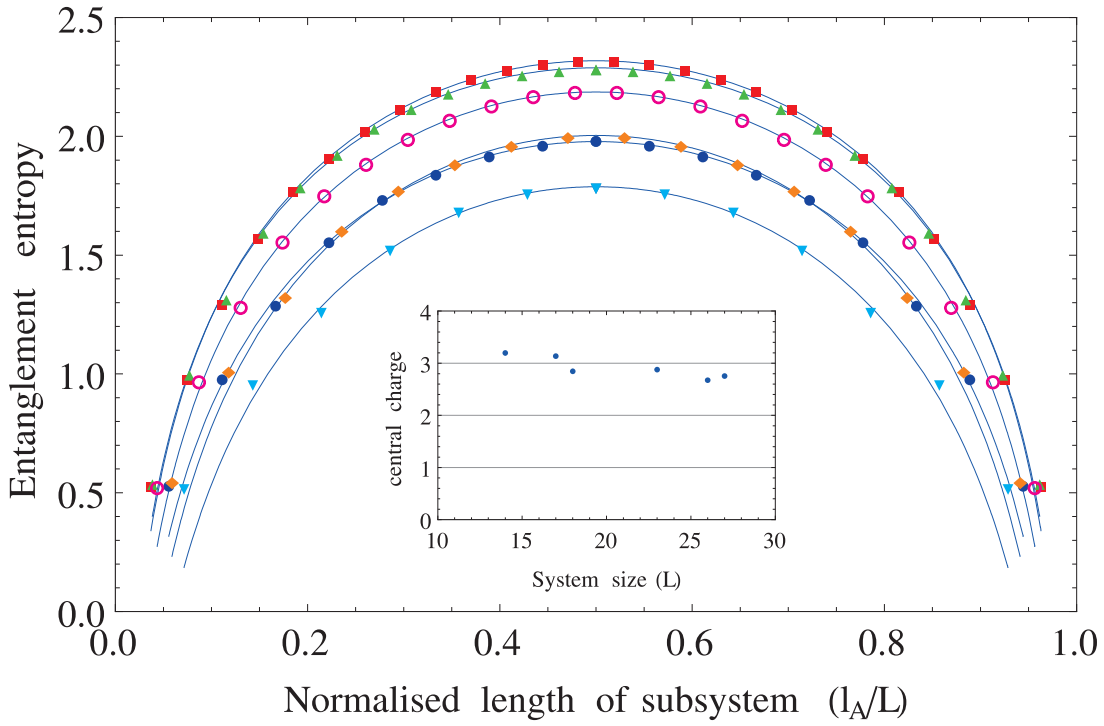

Figure 7.9: We plot the entanglement entropy for the states of the zig-zag ladder, which show critical behavior under spectral flow (see table 7.1). The entanglement entropy is plotted versus the number of sites (l_A) in the subsystem A normalized by the total number of sites (L). The total number of sites (L) and the number of fermions (f) of the systems we investigated are: $L(f) = 14(3), 17(4), 18(4), 23(5), 26(6), 27(6)$. The corresponding plot markers are from the middle outwards: triangles, diamonds, circles, open circles, triangles and squares. The inset in the middle shows the values of the central charge extracted from the fits to the entanglement entropy versus the total number of sites.

the system also shows charge ordering at 1/5 filling. In figure 7.11(a) we plot the one-point function for the ground state of the zig-zag ladder of 25 sites with open boundary conditions and 5 particles[2]. At first glance the charge ordering seems very clear, but we have to be careful. Remember that the one-point function for the supersymmetric model on the chain also showed this substructure reminiscent of charge order, which was shown to vanish in the continuum limit (see section 4.9.2). Here we would like to see that the charge ordering persists in the continuum limit. Unfortunately, at this point we do not have enough data to claim this, since there is a -very small[3]- decay of the peak as one moves into the bulk. Nevertheless, combining these findings with the results presented in the previous sections, there is little room for a different conclusion than that the system is charge ordered also at 1/5 filling.

These findings suggest that the ground states are dominated by the tilings, that is the particles in the state are confined to quantum fluctuate within a certain area set by

[2]We choose open boundary conditions, since for periodic boundary conditions the ground state at 1/5 filling is 5-fold degenerate. A numerically obtained wavefunction, will be an arbitrary superposition of these states and the one-point function for such a state does not give much insight. We can distinguish between the five ground states by imposing translational invariance, but this destroys any structure in the one-point function.

[3]There is less than 2% decay from the outer peaks to the middle peak for the system with 25 sites.

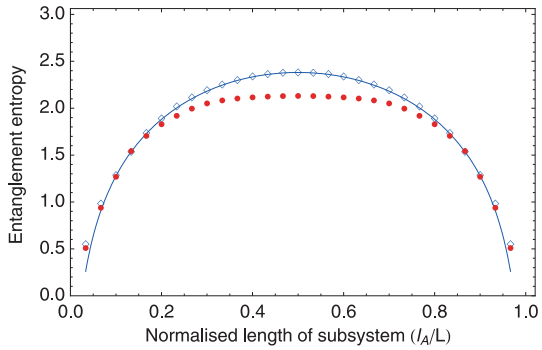

(a) $L = 30$, $f = 6$ (dots) and $f = 7$ (diamonds).

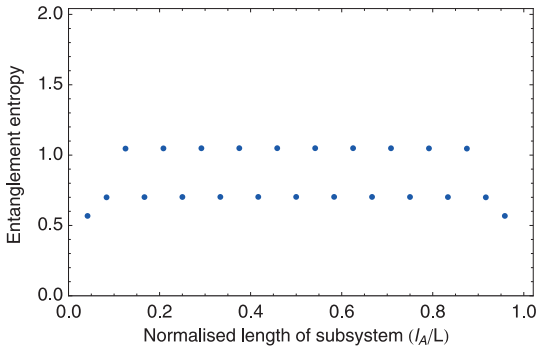

(b) $L = 24$, $f = 6$.

Figure 7.10: On the left we show the entanglement entropy (dots) for one of the 5 ground states of the zig-zag ladder with 30 sites at 1/5 filling ($f = 6$). For comparison we also plot the entanglement entropy (diamonds) of a ground state of the system with one extra fermion. Here the system is close to 2/9 filling and for the entanglement entropy there is a good fit with (7.10) (blue line). The zig-zag ladder with 30 sites and 7 particles has 92 zero energy ground states with periodic boundary conditions. To select one of these, we computed the entanglement entropy of the ground state for anti-periodic boundary conditions. On the right we plot the entanglement entropy for a ground state of the zig-zag ladder with 24 sites at 1/4 filling ($f = 6$). The ground states have momenta $p = \pi/2$ and $p = 3\pi/2$ and are both two-fold degenerate. It follows that we show the entanglement entropy of a certain superposition of the states $|\Psi_\alpha\rangle$ (7.8).

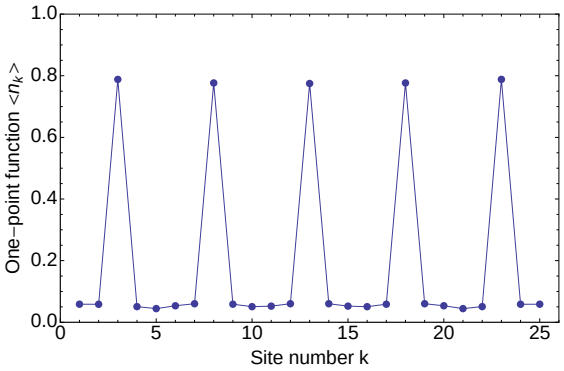

(a) $L = 25$, $f = 5$ and open boundary conditions.

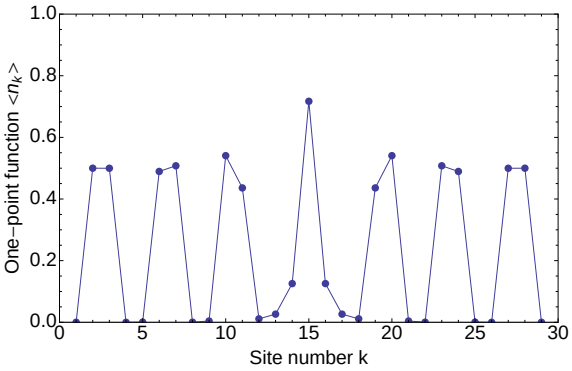

(b) $L = 29$, $f = 7$, periodic boundary conditions and perturbed hamiltonian.

Figure 7.11: On the left we plot the one-point function versus the site number for the ground state of the zig-zag ladder with 25 sites at 1/5 filling ($f = 5$) and open boundary conditions. On the right we plot the one-point function versus the site number for the ground state of the zig-zag ladder with 29 sites for $f = 7$ and periodic boundary conditions ($\vec{u} = (14, -1)$ and $\vec{v} = (1, 2)$). A small perturbation term is added to the supersymmetric hamiltonian: $H = \{Q, Q^\dagger\} - \epsilon c_{15}^\dagger c_{15}$, with $\epsilon = 0.01$, which favors site 15 to be occupied.

the tiles. To further test this idea, we compute the one-point function for the zig-zag ladder with 29 sites and 7 particles (see figure 7.11(b)). The tilings corresponding to the ground states of this system consist of 6 diamonds and one square. To select one specific tiling we add a small perturbation to the hamiltonian. By slightly changing the lattice

potential of one site, we favor this site to be occupied. This perturbation mildly breaks supersymmetry. From the one-point function of the ground state, we clearly see that this perturbation indeed seems to select the tiling with the square pinned to the perturbed site. Although, one should be careful interpreting this data, it is definitely in good agreement with the idea that the tiles set a certain area for the particles within which they can fluctuate. In particular, we can interpret the square tile as a defect in the charge ordered phase given by the diamonds. The fact that the one-point function corresponding to the quarter filled phase is recovered within a distance of 10 sites from the defect, suggests that this defect is indeed localized.

7.4.4 Flat band

For the zig-zag ladder there are zero-energy ground states at all rational filling fractions in the range between 1/5 and 1/4. For example, for a system with 30 sites there are 5 linearly independent ground states with 6 particles and 92 with 7 particles. In the previous sections we have seen that the tilings not only count, but indeed seem to dominate the actual ground states. From numerically inspecting one-point functions for specific ladder lengths, we have seen that the charge distribution of a ground state largely overlaps with that of the corresponding tiling. We can exploit this to gain physical insight. There are two uniform phases: all squares at 1/5 filling and all diamonds at 1/4 filling. One diamond in a phase with all squares is then a zero-energy defect with fractional charge 1/5. From counting the number of tilings with one such defect it follows that a defect can have any momentum. This is reminiscent of a flat band. Flat bands usually arise either from tuning the hopping terms of non-interacting particles on an exotic lattice, or from tuning potential terms for strongly interacting particles with negligible kinetic energy (see e.g. [86, 87] and references therein). Here, however, the flat band arises from tuning the potentials for particles with kinetic and potential energies of comparable size. Note that filling this flat band with defects is slightly subtle. Since defects cannot sit on top of each other and span over 4 sites, they obey a certain exclusion statistics.

7.4.5 Mapping to spin chain

In section 4.6.2 we briefly summarize the mapping between the supersymmetric model on the chain and the XXZ Heisenberg spin chain [23]. Borrowing these ideas, one can also find a mapping from the supersymmetric model on the zig-zag ladder to a spin chain. Similar to the chain, we map a site occupied by a fermion, including its four adjacent edges to a down-spin and the three edges between three empty sites to an up-spin (see figure 7.12). The length of the spin chain can therefore be written as $L = N - 2f$, where N is the number of sites in the zig-zag ladder and f the number of fermions. It follows from the mapping that a hop along a leg of the ladder corresponds to a spin flip between next-nearest neighbors, whereas a hop from one leg to the other corresponds to a spin flip between nearest neighbors. We thus find for the off-diagonal term in the supersymmetric model

$$\sum_i \left[P_{<i>} \left(c_i^\dagger c_{i+1} + c_{i+1}^\dagger c_i \right) P_{<i+1>} \right]$$
$$\Longleftrightarrow$$
$$\sum_j \left[\sigma_j^+ \sigma_{j+1}^- + \sigma_j^- \sigma_{j+1}^+ + \sigma_j^+ \sigma_{j+2}^- + \sigma_j^- \sigma_{j+2}^+ \right]$$

where the spin-flip operators are defined in terms of the usual Pauli matrices, $\sigma^{\pm} \equiv (\sigma^x \pm \imath\sigma^y)/2$. The diagonal term in the supersymmetric hamiltonian counts the number of empty next-nearest neighbor pairs, that is the number of sites (empty or occupied) surrounded by four empty sites. Under the mapping such a configuration either translates into a down-spin or into three neighboring up-spins. We thus find

$$\sum_i P_{<i>} \Longleftrightarrow \sum_j (1-\sigma_j^z)/2 + (1+\sigma_j^z)(1+\sigma_{j+1}^z)(1+\sigma_{j+2}^z)/8. \tag{7.11}$$

Working out the latter for a periodic spin chain of length L, we find

$$\sum_i P_{<i>} \Longleftrightarrow \frac{5L}{8} + \sum_{j=1}^{L} \left(-\frac{1}{4}\sigma_j^z + \frac{1}{4}\sigma_j^z\sigma_{j+1}^z + \frac{1}{8}\sigma_j^z\sigma_{j+2}^z + \frac{1}{8}\sigma_j^z\sigma_{j+1}^z\sigma_{j+2}^z \right). \tag{7.12}$$

Combining the results for the diagonal and off-diagonal terms we find that the supersymmetric model on the zig-zag ladder maps onto the following spin hamiltonian

$$\begin{aligned} H' &= \frac{1}{2}\sum_{j=1}^{L}\left[\sigma_j^x\sigma_{j+1}^x + \sigma_j^y\sigma_{j+1}^y + \frac{1}{2}\sigma_j^z\sigma_{j+1}^z\right] \\ &+ \frac{1}{2}\sum_{j=1}^{L}\left[\sigma_j^x\sigma_{j+2}^x + \sigma_j^y\sigma_{j+2}^y + \frac{1}{4}\sigma_j^z\sigma_{j+2}^z\right] \\ &- \frac{1}{4}\sum_{j=1}^{L}\sigma_j^z + \frac{1}{8}\sum_{j=1}^{L}\sigma_j^z\sigma_{j+1}^z\sigma_{j+2}^z + \frac{5L}{8}. \end{aligned} \tag{7.13}$$

We should warn the reader that this mapping is not one-to-one for the spectra. As for the chain the Hilbert spaces are not equal and one should account for the fermionic character of the particles in the supersymmetric model by imposing twisted boundary conditions in the spin chain.

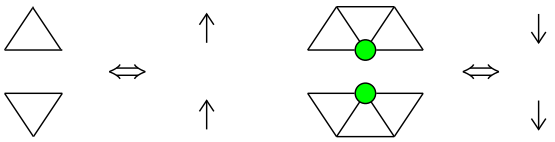

Figure 7.12: To map the supersymmetric model onto a spin chain, we identify a site occupied by a fermion, including its four adjacent edges to a down-spin and the three edges between three empty sites to an up-spin.

It is clear that the supersymmetric model on the zig-zag ladder maps to a rather involved and not very generic spin model. Nevertheless, it would be interesting to see if this relation can be exploited. In particular, it would be interesting to study the spin chain in the different sectors corresponding to different fillings in the supersymmetric model. In particular, the ground states at quarter filling map to a resonating valence bond state in the spin chain. These states are also known as the Majumdar-Ghosh states, which are known to be the ground states of a different, but related hamiltonian, namely the Majumdar-Ghosh hamiltonian [88]

$$H_{\mathrm{MG}} = \sum_i \left[\vec{S}_i \cdot \vec{S}_{i+1} + \frac{1}{2}\vec{S}_i \cdot \vec{S}_{i+2} \right]. \tag{7.14}$$

Interestingly, quarter filling precisely corresponds to zero magnetic field ($\sum_{j=1}^{L} \sigma_j^z = 2f - L = 4f - N = 0$). The largest number of ground states occurs at 2/9 filling, which thus corresponds to optimal frustration in the spin chain. Based on the spectral flow analysis presented in the next section, we strongly believe that the model is quantum critical at this filling. Finally, at one fifth filling the system is expected to be gapped again. In the spin chain this may thus correspond to a phase transition as a function of the external magnetic field. There is clearly still a lot of room for a better understanding of this model and the mapping to the spin chain may provide a way to make progress and, at the same time, be an incentive to pursue these issues further.

7.5 Square ladder

Of the ladder realization of the square lattice considered here, the ground state structure of the square ladder is clearly the simplest. The number of ground states is 3 if the total number of sites is a multiple of 8 and the ground state is unique otherwise. Note that this periodic substructure resembles that of the chain. In this section we will try to explore this resemblance, by carrying out a further analysis of the square ladder, analogous to the analysis carried out for the supersymmetric model on the chain (see section 4.7).
Remember that for the superconformal models in the minimal series the Witten index reads $W_k = k+1$. From the fact that the Witten index is 3 (for ladder lengths $L = 4j$), a first guess for the continuum theory is the second ($k = 2$) superconformal minimal model. This guess is further supported by the fact that the supersymmetric model on the square ladder can also be seen as the plus-minus model on the chain. The plus-minus model is the supersymmetric model with two types of particles ("+" and "−"). The supercharge reads $Q = Q_+ + Q_-$, where Q_+ (Q_-) is a sum over all sites of the creation operators of the "+"-particle ("−"-particle). Clearly if we interpret the particles on the upper leg of the square ladder as "+"-particles and the particles on the lower leg of the square ladder as "−"-particles, the two models are identical. This picture agrees with the idea that the continuum theory has central charge $c = 3/2$. The bosonic part corresponds to the charge degrees of freedom and the fermionic part to the 'spin' degrees of freedom. Finally, entanglement entropy computations for the square ladder with open bc give $c \approx 1.5$ [66].
In the following we will test this first guess in more detail. We will see that we encounter a number of difficulties. It is not clear if these issues are finite size effects, or if our first guess is incorrect. In the last section we discuss the possibility that the continuum theory is a different $c = 3/2$ theory. Thus far this issue remains unresolved. We are optimistic, however, that further advanced numerical studies of the system can be successful in identifying the continuum theory. Clearly, the fact that the simplest guess seems too simple, makes this project all the more worthwhile.

7.5.1 First guess for the continuum theory

In this section we will discuss the second ($k = 2$) superconformal minimal model. The second superconformal minimal model has central charge $c = 3/2$, which means that it consists of a boson ($c = 1$) and a fermion ($c = 1/2$). The boson can be compactified on a circle with radius R. At $R = \sqrt{2}$ the conformal algebra is extended to an $\mathcal{N} = 2$ superconformal algebra. At this point the $c = 3/2$ conformal field theory precisely matches

the second superconformal minimal model [47, 89]. As explained above this is our first guess for the continuum limit of the supersymmetric model on the square ladder. In the following we will test this idea by comparing the spectrum of the continuum theory with finite size spectra for both periodic as well as open boundary conditions, just as we did for the chain (see section 4.7).

Spectrum of the continuum theory

Let us start with the spectrum of the continuum theory. The partition function for the theory on the torus is composed of a bosonic part and a fermion part. The bosonic part for compactification radius r reads

$$\Gamma(r) = \frac{1}{\eta\overline{\eta}} \sum_{m,n\in Z} q^{\frac{1}{2}(m/2r+nr)^2} \overline{q}^{\frac{1}{2}(m/2r-nr)^2}, \tag{7.15}$$

where $q = e^{2\pi\imath\tau}$ (τ is the modular parameter for the torus) and

$$\eta = q^{1/24} \prod_{n=1}^{\infty} (1-q^n). \tag{7.16}$$

The fermionic part is given by

$$Z_{\text{Ising}} = \frac{1}{2}\left(\left|\frac{\theta_3}{\eta}\right| + \left|\frac{\theta_4}{\eta}\right| + \left|\frac{\theta_2}{\eta}\right|\right), \tag{7.17}$$

where

$$\begin{aligned}
\sqrt{\frac{\theta_3}{\eta}} &= q^{-1/48} \prod_{n=1}^{\infty} (1+q^{n-1/2}) \\
\sqrt{\frac{\theta_4}{\eta}} &= q^{-1/48} \prod_{n=1}^{\infty} (1-q^{n-1/2}) \\
\sqrt{\frac{\theta_2}{\eta}} &= \sqrt{2} q^{1/24} \prod_{n=1}^{\infty} (1+q^n).
\end{aligned} \tag{7.18}$$

The partition function for $r = \sqrt{2}$ reads

$$\begin{aligned}
Z_{\text{circ}}(\sqrt{2}) &= \Gamma(\sqrt{2}) Z_{\text{Ising}} \\
&= (q^{-1/16} + q^{15/16} + \dots)\overline{q}^{-1/16} + (3 + 4q + \dots) + \\
&\quad (2q^{1/16} + \dots)\overline{q}^{1/16} + (2q^{3/16} + \dots)\overline{q}^{3/16} + \\
&\quad (2q^{1/4} + \dots)\overline{q}^{1/4} + (q^{7/16} + \dots)\overline{q}^{7/16} + \\
&\quad (q^{1/2} + \dots)\overline{q}^{1/2} + \dots
\end{aligned} \tag{7.19}$$

Due to the conventions used here the powers of q and $\overline{q}$ correspond to the eigenvalues of $L_0 - 1/16$ and $\overline{L}_0 - 1/16$ respectively. The energy levels can thus be found from Z_{circ} by summing the powers of q and $\overline{q}$. We find the following energy levels

Energy	degeneracy	sector
-1/8	1	NS
0	3	R
1/8	2	NS
3/8	2	NS
1/2	2	R
7/8	1	NS
	...	

Let us check that this agrees with the spectrum of the second superconformal minimal model. The allowed conformal dimensions are (see section 3.4)

$$h = \frac{1}{16}, \frac{1}{16}, \frac{1}{16}, \frac{5}{16}, \frac{9}{16}, \frac{9}{16} \qquad \text{(R)}$$
$$h = 0, \frac{1}{8}, \frac{1}{8}, \frac{1}{4}, \frac{1}{4}, \frac{1}{2} \qquad \text{(NS)}.$$

For states with $h_L = h_R = h$ we thus find $E = 2h - 1/8$. For the first few values of the conformal dimensions this nicely reproduces the energies we obtained from the partition sum. The only subtlety is that the state with energy $E = 1/2$ is doubly degenerate in the Ramond sector, even though there is only one highest weight state with $h = 5/16$. The other state, however, can be obtained from this state using the supercharges. We also saw this for the first minimal model, where in the Ramond sector the non-zero energy highest weight state forms a quadruplet representation of the supersymmetry algebra (see section 4.7.1).

Finite size scaling

We now consider the finite size spectra. We will consider the supersymmetric model on the square ladder of length $L = 4j$. For this length the system has three zero energy ground states when we impose periodic boundary conditions. These should correspond to the three Ramond vacua. For ladder lengths $L \neq 4j$ the system has only one zero energy ground state for periodic boundary conditions and, as for the chain, we expect these to correspond to twisted sectors of the continuum theory. For ladders of up to 32 sites we compute the spectra for periodic and anti-periodic boundary conditions. An example is shown in figure 7.14. Remember that the finite size scaling of the numerically obtained energy is given by

$$E_{\text{num}} = 2\pi v_F E_{\text{CFT}}/L + \mathcal{O}(1/L^2), \tag{7.20}$$

where v_F is the Fermi velocity and L is the length of the system. So we can extract v_F from the energy of the Neveu-Schwarz vacuum for several system sizes and then determine the other energies, or conversely we can look at the ratios between the energy levels and the vacuum energy (E_0). We have computed the spectra for periodic and anti-periodic boundary conditions for ladders with 16, 24 and 32 sites and fitted each energy level as a function of the length to the function $E_{\text{num}} = a/L + b/L^3$ (an example is shown in figure 7.13). For the Neveu-Schwarz vacuum we obtain $a \approx -1.719$ which we define as a_0. For the other levels we show the results in table 7.2. Clearly, we do not find a good agreement.

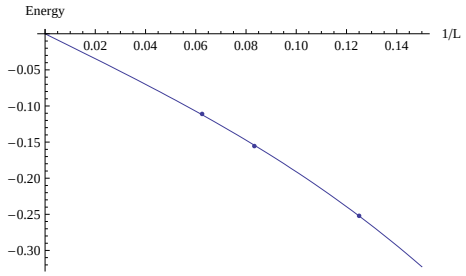

Figure 7.13: Energy of the NS vacuum plotted against $1/L$.

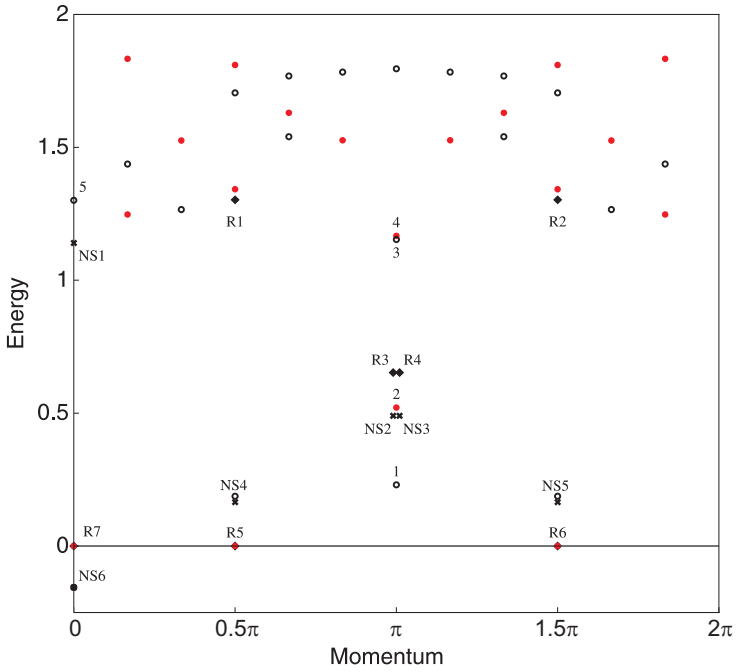

Figure 7.14: We show the spectra of the supersymmetric model on the square ladder with 24 sites and 6 particles for periodic and anti-periodic boundary conditions. The spectrum for (anti-) periodic boundary conditions is given by the red filled (black open) circles. The diamonds are highest weight states in the Ramond sector, the crosses are highest weight states in the NS sector (both are scaled with a fitted Fermi velocity according to (7.20))

Spectral flow: avoided level crossings

Let us now look at the spectral flow analysis for the square ladder. In figure 7.15 we plot the spectra for twist parameter α between 0 and 1, with steps of 1/8. The discrepancy between the finite size scaling and the continuum spectrum can now be interpreted as an avoided level crossing as a function of the twist parameter. Remember that we also saw avoided crossings on the chain, however, in that case they were shown to vanish in the continuum limit (see section 4.8.1). Here the scaling analysis seems to suggest that the avoided crossing persists in the continuum limit.

Table 7.2: The first column gives the level labels corresponding to the labels in figure 7.14. The second column gives the ratio of the energy to the vacuum energy in the continuum theory (second superconformal minimal model). The third column gives the ratio of the fitted value for the energy to the fitted value for the vacuum energy. The last column gives the ratio of the energy to the vacuum energy in the continuum theory with $c = 3/2$, but now the orbifold line (see section 7.5.2).

Label	Theory E_{CFT}/E_0 ($r_{\mathrm{circ}} = \sqrt{2}$)	Fitted a/a_0	Theory E_{CFT}/E_0 ($r_{\mathrm{orb}} = 1$)
NS6	1	1	1
NS4(=NS5)	-1	-1.17	-1
1	-3	-1.54	-1
2	-4	-3.27	-2
3	-3	-8.34	-7
4	-4	-7.58	-8
5	-7	-11.20	-7

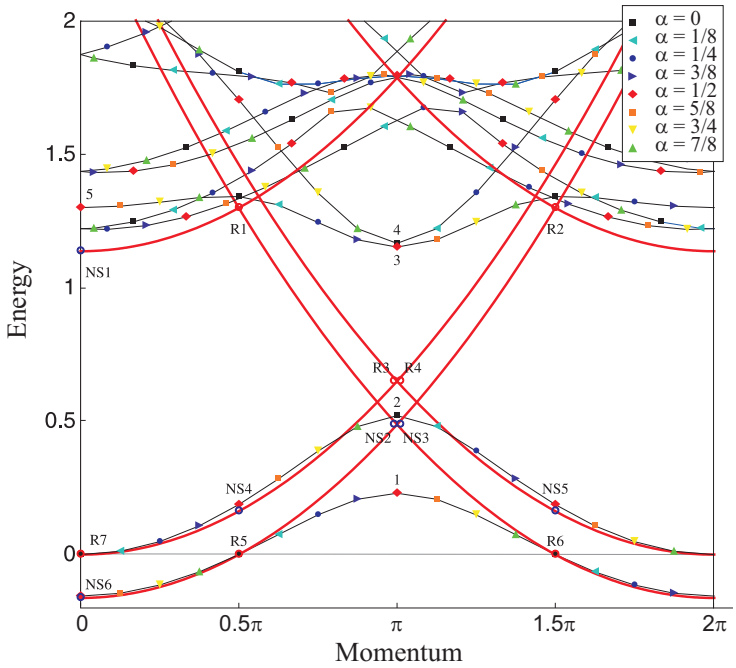

Figure 7.15: We plot the spectra for twist parameter α between 0 and 7/8, with steps of 1/8. The black line connects the levels for different values of the twist parameter. The red lines are the theoretical prediction for the spectral flow, open red circles correspond to the Ramond sector ($\alpha \in \mathbb{Z}$) and open blue circles correspond to the Neveu-Schwarz sector ($\alpha \in \mathbb{Z} + 1/2$).

Open boundary conditions

For the square ladder with open boundary conditions we expect that the left- and right-moving modes are coupled, just as was found for the chain in section 4.9.1. In this section, we consider again our first guess for the continuum theory, namely the second superconformal minimal model. We first compute the spectrum of the continuum theory with coupled left- and right-moving modes and then compare this with the numerical analysis of the

finite size spectra of the lattice model. The boson compactified on a circle with radius $r = \sqrt{2}$ is represented by the operators

$$\Phi_m = e^{\imath m\phi/\sqrt{2}}, \tag{7.21}$$

with conformal dimension

$$h_m = m^2/4. \tag{7.22}$$

For the fermion we have the trivial representation 1, the fermion ψ and the twist-field σ, with conformal dimensions $h_1 = 0$, $h_\psi = 1/2$ and $h_\sigma = 1/16$ respectively. The supercharges are given by

$$G^{\pm} = \psi e^{\pm\imath\sqrt{2}\phi}, \tag{7.23}$$

with conformal dimension $h = 1/2 + 1 = 3/2$.
Supersymmetry in the lattice model tells us that we are in the Ramond sector. There we have the following operator content: Φ_m and $\psi\Phi_m$ with $m \in Z+1/2$ and $\sigma\Phi_m$ with $m \in Z$. There are three highest weight states with zero energy, $\sigma\Phi_0$ and $\Phi_{\pm 1/2}$. The degeneracies of the levels generated from the highest weight states by the Virasoro algebra are given by

$$\begin{aligned}
\prod_{n=1}^{\infty}(1-q^n)^{-1}\prod_{j\geq 1}(1+q^j) &= 1 + 2q + 4q^2 + 8q^3 + 14q^4 + \ldots \text{ and} \\
\prod_{n=1}^{\infty}(1-q^n)^{-1}\prod_{j\geq 0}(1+q^{j+1/2}) &= 1 + q^{1/2} + q + 2q^{3/2} + 3q^2 + 4q^{5/2} + \ldots
\end{aligned} \tag{7.24}$$

in the sector with and without twistfield respectively. We can now construct the spectrum for $H = L_0 - c/24 = L_0 - 1/16$ as a function of m (see figure 7.16).
Since the supercharge increases m by two, we can make the following identification

$$\tilde{f} \equiv f - L/2 = (m + 1/2)/2, \tag{7.25}$$

where L is the total number of rungs of the square ladder. In figure 7.17 we plot the sector for which $\tilde{f} = 0$, i.e. $m = 3/2 \mod 2$. The other sector present in the lattice model is $\tilde{f} = 1/2$, i.e. $m = 1/2 \mod 2$ (the blue spectrum in figure 7.16).
The sectors with twist field will probably correspond to the ladder with an odd number of sites. For $N = 4n + 1$, where N is the number of sites, we find that the Witten index is zero. On the other hand, for $N = 4n - 1$ we find $|W| = 1$. If we compare this with (7.25), we find that the $m = 0$ sector (the black spectrum in figure 7.16) corresponds to $N = 4n - 1$ with $f = n$, whereas $m = 1$ and $m = -1$ (the yellow spectrum in figure 7.16) correspond to $N = 4n + 1$ with $f = n$ and $f = n + 1$ respectively.
In an unfinished study, we compared these finding to numerical data obtained with DMRG methods [66]. Preliminary results show similar issues as for periodic boundary conditions. In contrast with the results obtained for the chain with open boundary conditions (see figure 4.11), the spectra seem to contain various scales even for large system sizes. Furthermore, we investigated how the energy of the ground state depends on the fermion number.

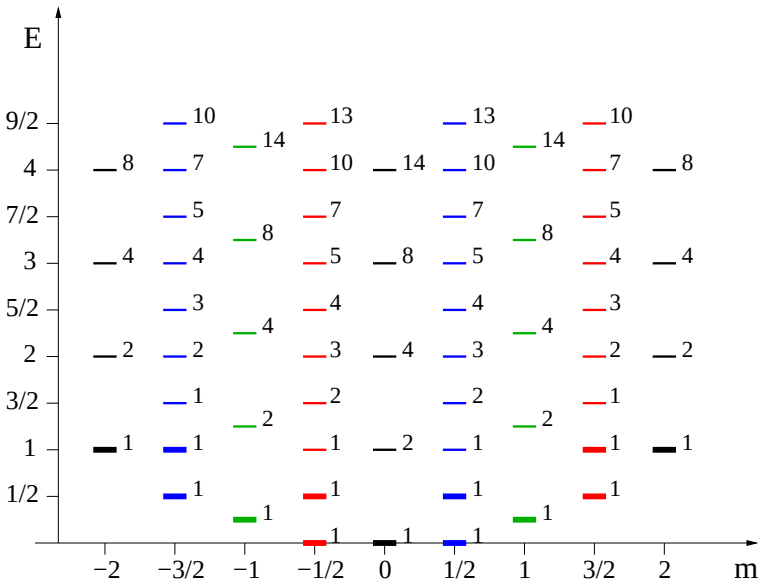

Figure 7.16: We show the spectrum of the second superconformal minimal model with $\mathcal{N} = 2$ supersymmetry. The energy $E = h - 1/16$ is plotted versus m. The level corresponding to the primary field and the levels that are generated from this field by the supercharge operators are indicated by a thick bar. The descendants are indicated by thinner bars. The label indicates the degeneracy of the levels. The color distinguishes sectors with different values for $m \mod 2$.

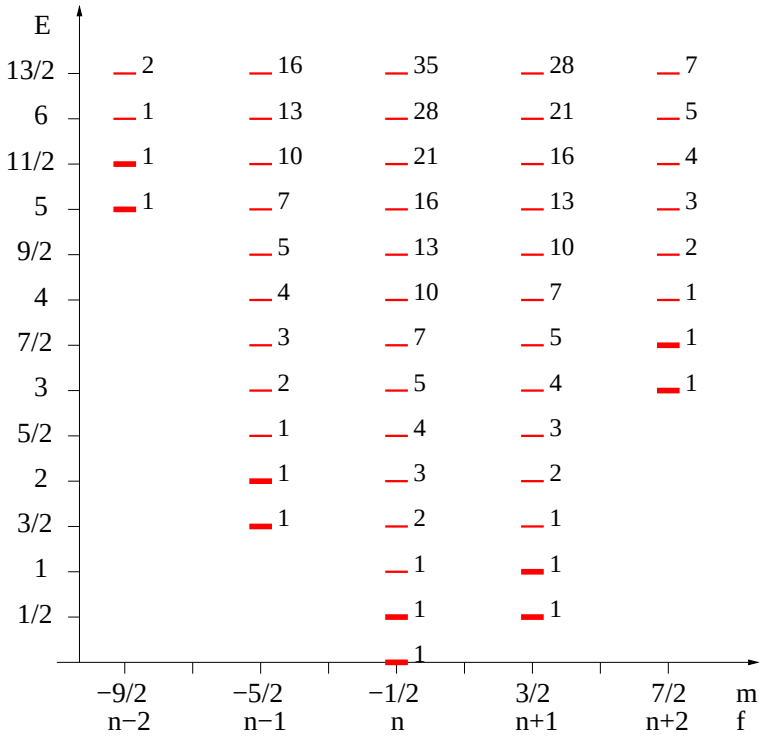

Figure 7.17: We show one sector of the spectrum of the second superconformal minimal model with $\mathcal{N} = 2$ supersymmetry.The energy $E = h - 1/16$ is plotted versus m for $m = 3/2 \mod 2$, corresponding to a ladder with an even number of rungs $L = 2n$.

In the continuum theory we have $E = h_m - c/24 = m^2/(2r^2) - c/24$, which suggests a

parabolic dependence. Now let us define m_0 as follows: $m \equiv F - F_{GS} + m_0$, Since the energy is zero at $F = F_{GS}$, we find

$$\frac{m_0^2}{2r^2} = \frac{c}{24} \tag{7.26}$$

and thus

$$E_{GS}L = \frac{v_F \pi}{2r^2}\big((F - F_{GS})^2 + 2(F - F_{GS})m_0\big). \tag{7.27}$$

So $E_{GS}L$ should give a nice fit with $a(F - F_{GS})^2 + b(F - F_{GS})$. It follows that $b/a = 2m_0$, so we can extract m_0.
Upon comparison with the numerics, however, we find that such a fit does not seem to work well. Instead a much better fit is obtained when fitting E for $F < F_{GS}$ and $F > F_{GS}$ separately. This is quite puzzling and suggests that the lack of a particle-hole symmetry in the lattice model may be at the source of all the discrepancies we find. To determine whether the lack of this symmetry just causes very persistent finite size effects or that the continuum theory is truly different is still an open question.

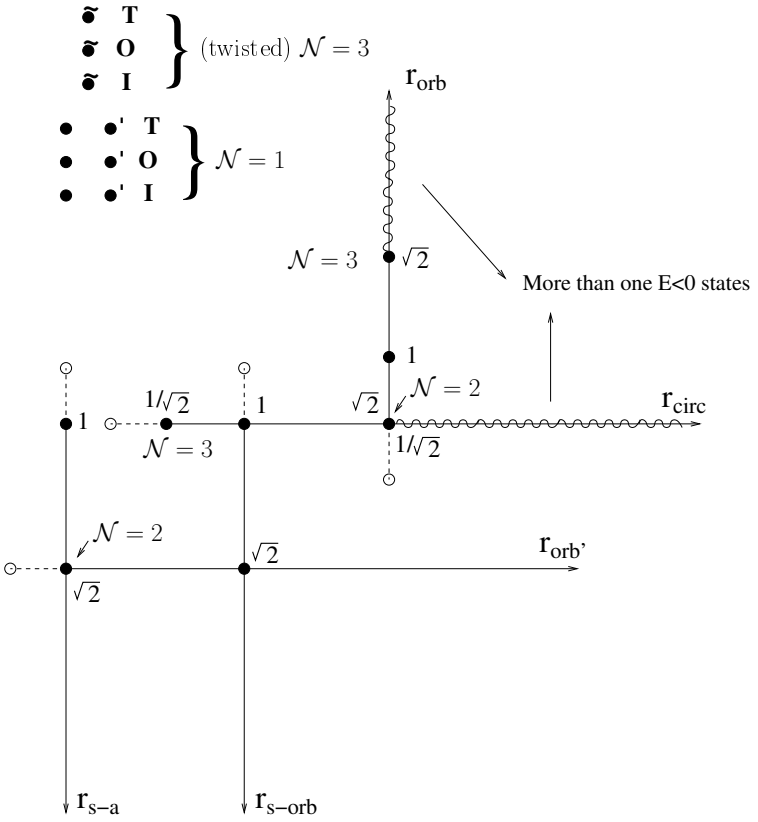

Figure 7.18: Survey of the $c = 3/2$ theories.

7.5.2 Other $c = 3/2$ theories

The superconformal minimal model with $k = 2$ is one of the theories with central charge $c = 3/2$. A survey of the $c = 3/2$ theories is given by Dixon, Ginsparg and Harvey in

[89] and is schematically depicted in figure 7.18. The second minimal model lies on the circle line at radius $r_{\text{circ}} = \sqrt{2}$. As we have seen, this theory is a promising candidate to describe the continuum limit of the square ladder, however, it runs into some trouble. Here we consider several other candidates and check a number of properties. The theory should have at least $\mathcal{N} = 2$ supersymmetry, three Ramond vacua and one negative energy state in the Neveu-Schwarz sector. Finally, for the theories on the orbifold line, we compare the higher energy states with the scaling analysis of the finite size spectra.
The following theories have at least $\mathcal{N} = 2$ supersymmetry.

- **The $\mathcal{N} = 2$ SUSY point on the super affine line**
  The $\mathcal{N} = 2$ supersymmtric point on the super affine line sits at $r = \sqrt{2}$. Its partition function is given in [89]. However, there are no zero energy states in the spectrum.
- **The $\mathcal{N} = 3$ SUSY point on the circle line at $r = 1/\sqrt{2}$**
  The $\mathcal{N} = 3$ supersymmtric point on the circle line at $r = 1/\sqrt{2}$ has just one zero energy state.
- **The (twisted) $\mathcal{N} = 3$ SUSY points $\tilde{T}$, $\tilde{O}$, $\tilde{I}$**
  The (twisted) $\mathcal{N} = 3$ supersymmtric points $\tilde{T}$, $\tilde{O}$ and $\tilde{I}$ have respectively 2, 3 and 2 zero-energy states and there are 3, 3 and 4 negative energy states respectively.
- **The (twisted) $\mathcal{N} = 3$ SUSY points on circle line with $r = n/\sqrt{2}$**
  The first two (twisted) $\mathcal{N} = 3$ supersymmtric points on the circle line sit at $r = 1/\sqrt{2}$, $r = \sqrt{2}$ and correspond to the second minimal model and its dual. For $n > 2$, we find $r^2/2 = n^2/4 > 1$ and thus there is more than one negative energy state (see the partition sum for the circle line (7.15)).

On the orbifold line there are three Ramond vacua, but the $\mathcal{N} = 2$ supersymmetry is broken to an $\mathcal{N} = 1$ supersymmetry. For certain values of the compactification radius, however, it is enhanced to $\mathcal{N} = 3$. The partition function on the orbifold line reads

$$Z_{\text{orb}}(r) = \frac{1}{2}(\Gamma(r) + \frac{|\theta_3\theta_4|}{\eta\overline{\eta}} + \frac{|\theta_2\theta_3|}{\eta\overline{\eta}} + \frac{|\theta_2\theta_4|}{\eta\overline{\eta}})Z_{\text{Ising}}. \tag{7.28}$$

The first terms of the r-independent part read

$$\begin{aligned}\frac{1}{2}(q\overline{q})^{-1/16} + \frac{5}{2} + 2(q\overline{q})^{1/16} + \frac{1}{2}(q\overline{q})^{7/16} + 4(q\overline{q})^{1/2} + \dots \\ -\frac{1}{2}(q^{15/16}\overline{q}^{-1/16} + h.c.) + 2(q + \overline{q}) + \dots\end{aligned} \tag{7.29}$$

The first terms of the r-dependent part read

$$\begin{aligned}\frac{1}{2}Z_{\text{Ising}}\Gamma(r) &= \Big(\frac{1}{2}(q\overline{q})^{-1/16} + \frac{1}{2} + \frac{1}{2}(q\overline{q})^{7/16} + \dots + \frac{1}{2}(q^{15/16}\overline{q}^{-1/16} + h.c.) \\ &\quad +(q + \overline{q}) + \dots\Big) * \sum_{m,n\in Z} q^{\frac{1}{2}(m/2r+nr)^2}\overline{q}^{\frac{1}{2}(m/2r-nr)^2} \\ &= \frac{1}{2}(q\bar{q})^{-1/16} + \frac{1}{2}(q\bar{q})^{0} + \frac{1}{2}(q\bar{q})^{7/16} \\ &\quad + \dots + \frac{1}{2}(q^{15/16}\overline{q}^{-1/16} + h.c.) + (q + \overline{q}) + \dots \\ &\quad +(q\bar{q})^{-1/16+1/(8r^2)} + (q\bar{q})^{1/(8r^2)} + (q\bar{q})^{7/16+1/(8r^2)} \\ &\quad +(q\bar{q})^{-1/16+r^2/2} + (q\bar{q})^{r^2/2} + (q\bar{q})^{7/16+r^2/2} + \dots\end{aligned}$$

So we obtain

$$\begin{aligned} Z_{\rm orb}(r) &= (q\bar{q})^{-1/16} + 3 + 2(q\bar{q})^{1/16} + (q\bar{q})^{7/16} + 4(q\bar{q})^{1/2} + \dots \\ &\quad +3(q+\bar{q}) + \dots + (q\bar{q})^{-1/16+1/(8r^2)} + (q\bar{q})^{1/(8r^2)} + (q\bar{q})^{7/16+1/(8r^2)} \\ &\quad +(q\bar{q})^{-1/16+r^2/2} + (q\bar{q})^{r^2/2} + (q\bar{q})^{7/16+r^2/2} + \dots \end{aligned} \tag{7.30}$$

We see that the levels that did not fit the finite size spectra are now r-dependent, except for the non-degenerate level with energy 7/8. The best fit follows from $r = 1$ (see table 7.2, last column), however there is just an $\mathcal{N} = 1$ SUSY at this point, which is not enough. The first $\mathcal{N} = 3$ SUSY point on the orbifold line occurs at $r = \sqrt{2}$, however there we find four Ramond vacua. For even larger radii there is more than one negative energy state. These negative energy states come from combining the first term in $Z_{\rm Ising}$ ($(q\bar{q})^{-1/48}$) with the first terms in $\Gamma(r)$, with m small and $n = 0$ for larger values of r:

$$(q\bar{q})^{-1/48}(q\bar{q})^{-1/24} \sum_{m\in Z} q^{\frac{1}{2}(m/2r)^2} \bar{q}^{\frac{1}{2}(m/2r)^2}. \tag{7.31}$$

These have negative energy when $m^2 < r^2/2$.
We conclude that none of the theories considered in this section is a convincing candidate for the continuum theory of the square ladder. In particular, none of them seems to do better than our first guess, the theory on the circle line with $r_{\rm circ} = \sqrt{2}$. Identifying the low energy continuum theory of the supersymmetric model on the square ladder thus stands as an open problem.